# A Variational Model for the Joint Recovery of the Fundamental Matrix and the Optical Flow

Levi Valgaerts, Andrés Bruhn, and Joachim Weickert

Mathematical Image Analysis Group
Faculty of Mathematics and Computer Science, Building E1.1
Saarland University, 66041 Saarbrücken, Germany
{valgaerts,bruhn,weickert}@mia.uni-saarland.de

**Abstract.** Traditional estimation methods for the fundamental matrix rely on a sparse set of point correspondences that have been established by matching salient image features between two images. Recovering the fundamental matrix from dense correspondences has not been extensively researched until now. In this paper we propose a new variational model that recovers the fundamental matrix from a pair of uncalibrated stereo images, and simultaneously estimates an optical flow field that is consistent with the corresponding epipolar geometry. The model extends the highly accurate optical flow technique of Brox *et al.* (2004) by taking the epipolar constraint into account. In experiments we demonstrate that our approach is able to produce excellent estimates for the fundamental matrix and that the optical flow computation is on par with the best techniques to date.

## 1 Introduction

The fundamental matrix is the basic representation of the geometric relation that underlies two views of the same scene. This relation is expressed by the so called epipolar constraint [5, 11], which tells us that corresponding points in the two views are restricted to lie on specific lines rather than anywhere in the image plane. A reliable estimation of the fundamental matrix from the epipolar constraint is essential for many computer vision tasks such as the 3D reconstruction of a scene, structure-from-motion and camera calibration.

Apart from a limited number of approaches that recover the fundamental matrix directly from image information [18], most methods are based on the prior determination of point correspondences. Of the latter type *feature-based methods* have proven to be very successful and are by far most frequently used. These methods try to match characteristic image features in the two views and compute the fundamental matrix by imposing the epipolar constraint on this sparse set of correspondences. Theoretically eight perfect point matches are sufficient to compute the fundamental matrix in a linear way [10]. In practice, however, the establishment of feature correspondences is error prone because the local nature of most feature-matching algorithms results in localization errors and false matches. This has led to the development of a multitude of robust extensions that can deal with a relatively large amount of outliers. M-estimators [9], Least Median of Squares [16] and the Random Sample Consensus (RANSAC) [6] number among such robust techniques.

Recent advances in optical flow computation have proven that variational methods are a viable alternative to feature-based methods when it comes down to the accuracy of the correspondences established between two images. In [12] the authors advocate the use of variational optical flow methods as a basis for the estimation of the fundamental matrix. The proposed approach offers at least two advantages over feature-based approaches: *(i)* Dense optical flow provides a very large number of correspondences and *(ii)* the amount of outliers is small due to the combination of a robust data term and a global smoothness constraint. Because of this inherent robustness no involved statistics was used in the estimation process and favorable results have been produced by using a simple least squares fit.

In this paper we propose a novel variational approach that allows for a simultaneous estimation of both the optical flow and the fundamental matrix. This is achieved by minimizing a joint energy functional. Our method extends the method of Brox *et al.* [3] by including the epipolar constraint as a soft constraint. In this context it differs from the two-step method proposed in [12] that concentrates solely on the estimation of the fundamental matrix from the optical flow. This has the disadvantage that the found correspondences are not corrected by the recovered epipolar geometry. Moreover, displacement fields that yield a good fundamental matrix are not necessarily good by optical flow standards. These observations clearly motivate a joint solution of both unknowns. Our strategy also differs from the work presented in [19], that focuses on the calculation of the disparity while imposing the epipolar constraint as a hard constraint. This work gave excellent results for the ortho-parallel camera setup but required the epipolar geometry to be known in advance.

Our method is related to other recent attempts to pair the epipolar constraint with other constraints such as the brightness constancy assumption in one joint formulation [18, 17]. However, these techniques are restricted to the estimation of non-dense correspondences. Close in spirit are also feature-based methods that minimize some type of reprojection error in which both the fundamental matrix and a new set of correspondences are estimated from an initial set of feature matches [5, 7].

Our paper is organized as follows. In Section 2 we shortly revise the estimation of the fundamental matrix from a set of correspondences. In Section 3 we introduce our variational model before discussing the minimization of the energy and the solution of the resulting equations. A performance evaluation is presented in Section 4, followed by conclusions and a summary in Section 5.

## 2 From Epipolar Constraint to Fundamental Matrix

The epipolar constraint between a given point $\tilde{\mathbf{x}} = (x, y, 1)^\top$ in the left image and its corresponding point $\tilde{\mathbf{x}}' = (x', y', 1)^\top$ in the right image can be rewritten as the product of two $9 \times 1$ vectors [5]:

$$0 = \tilde{\mathbf{x}}'^\top F \, \tilde{\mathbf{x}} = \mathbf{s}^\top \mathbf{f}, \tag{1}$$

where $\mathbf{s} = (xx',\, yx',\, x',\, xy',\, yy',\, y',\, x,\, y,\, 1)^\top$ and $\mathbf{f} = (f_{11},\, f_{12},\, f_{13},\, f_{21},\, f_{22},\, f_{23},\, f_{31},\, f_{32},\, f_{33})^\top$. Here $f_{i,j}$ with $1 \leq i, j \leq 3$ are the unknown entries of the fundamental matrix $F$ and the tilde superscript indicates that we are using projective coordinates.

To find the entries of $F$ from $n > 8$ point correspondences we can minimize the energy

$$\mathcal{E}(\mathbf{f}) = \sum_{i=1}^{n} (\mathbf{s}_i^\top \mathbf{f})^2 = \|S\,\mathbf{f}\|^2, \tag{2}$$

where $S$ is an $n \times 9$ matrix of which the rows are made up by the constraint vectors $\mathbf{s}_i^\top,\ 1 \leq i \leq n$. This is equivalent to finding a least squares solution to the over determined system $S\,\mathbf{f} = \mathbf{0}$. Since $F$ is defined up to a scale factor we can avoid the trivial solution $\mathbf{f} = \mathbf{0}$ by imposing the explicit side constraint on the norm $\|\mathbf{f}\|^2 = 1$. The solution of the thus obtained *total least squares (TLS)* problem [10] is known to be the eigenvector that belongs to the smallest eigenvalue of $S^\top S$.

The TLS method can be rendered more robust with respect to outliers by replacing the quadratic penalization in the energy (2) by another function of the residual:

$$\mathcal{E}(\mathbf{f}) = \sum_{i=1}^{n} \varPsi\left((\mathbf{s}_i^\top \mathbf{f})^2\right). \tag{3}$$

Here $\varPsi(s^2)$ is a positive, symmetric and in general convex function in $s$ that grows sub-quadratically, like for instance the regularized $L_1$ norm. Applying the method of Lagrange multipliers to the problem of minimizing the energy (3) with the constraint $\|\mathbf{f}\|^2 = \mathbf{f}^\top \mathbf{f} = 1$ means that we are looking for critical points of

$$\mathcal{F}(\mathbf{f}, \lambda) = \sum_{i=1}^{n} \varPsi\left((\mathbf{s}_i^\top \mathbf{f})^2\right) + \lambda(1 - \mathbf{f}^\top \mathbf{f}). \tag{4}$$

Setting the derivatives of $\mathcal{F}(\mathbf{f}, \lambda)$ with respect to $\mathbf{f}$ and $\lambda$ to zero finally yields the non-linear problem

$$\mathbf{0} = \left(\sum_{i=1}^{n} \varPsi'\left((\mathbf{s}_i^\top \mathbf{f})^2\right) \mathbf{s}_i \mathbf{s}_i^\top - \lambda I\right) \mathbf{f} = \left(S^\top\, W(\mathbf{f})\, S - \lambda I\right) \mathbf{f}\,, \tag{5}$$

$$0 = 1 - \|\mathbf{f}\|^2. \tag{6}$$

In the above formula $W$ is an $n \times n$ diagonal matrix with positive weights $w_{ii} = \varPsi'\left((\mathbf{s}_i^\top \mathbf{f})^2\right)$. To solve this nonlinear system we propose a lagged iterative scheme in which we fix the symmetric positive definite system matrix $S^\top W S$ for a certain estimate $\mathbf{f}^k$. This will result in a similar eigenvalue problem as in the case of the TLS fit, and by solving it for $\mathbf{f}^{k+1}$ we can successively refine the current estimate.

An important preliminary step aimed at improving the condition number of the eigenvalue problem is the normalization of the point data in the two images before the estimation of $F$. The points $\tilde{\mathbf{x}}$ and $\tilde{\mathbf{x}}'$ are transformed by the respective affine transformations $T$ and $T'$ such that $T\tilde{\mathbf{x}}$ and $T'\tilde{\mathbf{x}}'$ will have on average the projective coordinate $(1, 1, 1)^\top$. The fundamental matrix $\hat{F}$, estimated from the transformed points, is then used to recover the original matrix as $F = T'^\top\ \hat{F}\ T$. Data normalization was strongly promoted by Hartley in conjunction with simple linear methods [8]. Another issue concerns the rank of $F$. The estimates obtained by the minimization techniques presented in this section will in general not satisfy the rank 2 constraint. Therefore, it is common to enforce the rank of $F$ after estimation by e.g. singular value decomposition [5].

## 3 The Variational Model

In this section we will adopt the notations that are commonly used in variational optical flow computation. We assume that the two stereo images under consideration are consecutive frames in an image sequence $I(x, y, t) : \Omega \times [0, \infty) \rightarrow \mathbb{R}$. We denote by $\mathbf{x} = (x, y, t)^\top$ a location within the rectangular image domain $\Omega \in \mathbb{R}^2$ at a time $t \geq 0$. Our goal is to estimate the fundamental matrix $F$ together with the optical flow $\mathbf{w} = (u, v, 1)^\top$ between the left frame $I(x, y, t)$ and the right frame $I(x, y, t+1)$ of an uncalibrated pair of stereo images.

### 3.1 Integrating the Epipolar Constraint

In order to estimate the optical flow and the fundamental matrix jointly, we propose to extend the 2D variant of the model of Brox *et al.* [3] with an extra term as follows

$$\begin{aligned}\mathcal{E}(\mathbf{w}, \mathbf{f}) = \quad & \int_\Omega \Psi_d \left( |I(\mathbf{x} + \mathbf{w}) - I(\mathbf{x})|^2 + \gamma \cdot |\nabla I(\mathbf{x} + \mathbf{w}) - \nabla I(\mathbf{x})|^2 \right) \mathrm{d}x \, \mathrm{d}y \\ & + \alpha \int_\Omega \Psi_s \left( |\nabla \mathbf{w}|^2 \right) \mathrm{d}x \, \mathrm{d}y \, + \, \beta \int_\Omega \Psi_e \left( \left( \mathbf{s}^\top \, \mathbf{f} \right)^2 \right) \mathrm{d}x \, \mathrm{d}y, \end{aligned} \tag{7}$$

while imposing the explicit side constraint $\|\mathbf{f}\|^2 = 1$. Here $|\nabla \mathbf{w}|^2 := |\nabla u|^2 + |\nabla v|^2$ denotes the squared magnitude of the spatial flow gradient with $\nabla = (\partial_x, \partial_y)^\top$. The first term of $\mathcal{E}(\mathbf{w}, \mathbf{f})$ is the data term. It models the constancy of the image brightness and the spatial image gradient along the displacement trajectories. These two constraints combined provide robustness against varying illumination while their formulation in the original nonlinear form allows for the handling of large displacements. The second term is the smoothness term and it penalizes deviations of the flow field from piecewise smoothness. For the functions $\Psi_d(s^2)$ and $\Psi_s(s^2)$ the regularized $L_1$ penalizer $\Psi(s^2) = \sqrt{s^2 + \epsilon^2}$ is chosen which equals total variation (TV) regularization in the case of the smoothness term. While the first two terms in $\mathcal{E}(\mathbf{w}, \mathbf{f})$ are the same as in the original model, the newly introduced third term penalizes deviations from the epipolar geometry. The vectors $\mathbf{s}$ and $\mathbf{f}$ are defined as in Section 2 but this time $\mathbf{s}$ is a function of $\mathbf{x}$ and $\mathbf{w}$. To minimize the influence of outliers in the computation of $F$ we choose $\Psi_e(s^2)$ to be the regularized $L_1$ penalizer. The weight $\beta$ determines to what extend the epipolar constraint will be satisfied in all points. The constraint on the Frobenius norm of $F$ avoids the trivial solution.

### 3.2 Minimization

To minimize $\mathcal{E}(\mathbf{w}, \mathbf{f})$ with respect to $u$, $v$ and $\mathbf{f}$, subject to the constraint $\|\mathbf{f}\|^2 = 1$, we use the method of the Lagrange multipliers. We are looking for critical points of

$$\mathcal{F}(\mathbf{w}, \mathbf{f}, \lambda) = \mathcal{E}(\mathbf{w}, \mathbf{f}) + \lambda(1 - \mathbf{f}^\top \mathbf{f}), \tag{8}$$

i.e. tuples $(u^*, v^*, \mathbf{f}^*, \lambda^*)$ for which the functional derivatives of the Lagrangian $\mathcal{F}$ with respect to $u$ and $v$ and the derivatives of $\mathcal{F}$ with respect to $\mathbf{f}$ and $\lambda$ vanish:

$$0 = \frac{\delta}{\delta u} \mathcal{F}(\mathbf{w}, \mathbf{f}, \lambda), \quad 0 = \frac{\delta}{\delta v} \mathcal{F}(\mathbf{w}, \mathbf{f}, \lambda), \quad \mathbf{0} = \nabla_{\mathbf{f}} \, \mathcal{F}(\mathbf{w}, \mathbf{f}, \lambda), \quad 0 = \frac{\partial}{\partial \lambda} \mathcal{F}(\mathbf{w}, \mathbf{f}, \lambda). \tag{9}$$

Here $\nabla_{\mathbf{f}}$ stands for the gradient operator $\left(\frac{\partial}{\partial f_{11}}, \cdots, \frac{\partial}{\partial f_{33}}\right)^{\top}$.

The first two equations in equation system (9) are the Euler-Lagrange equations of the optical flow components $u$ and $v$. To derive them in more detail we first write the epipolar constraint as follows:

$$\mathbf{s}^{\top}\mathbf{f} = \begin{pmatrix} x+u \\ y+v \\ 1 \end{pmatrix}^{\top} F \begin{pmatrix} x \\ y \\ 1 \end{pmatrix} = \begin{pmatrix} u \\ v \\ 1 \end{pmatrix}^{\top} \begin{pmatrix} a \\ b \\ q \end{pmatrix} = a\,u + b\,v + q. \tag{10}$$

This is a scalar product involving the optical flow $\mathbf{w}$ where $a$ and $b$ denote the first two coefficients of the epipolar line $F\tilde{\mathbf{x}}$ of a point $\tilde{\mathbf{x}} = (x, y, 1)^{\top}$ in the left image. The quantity $q = \tilde{\mathbf{x}}^{\top} F\, \tilde{\mathbf{x}}$ can be interpreted as the distance of $\tilde{\mathbf{x}}$ to its own epipolar line up to the normalization factor $1/\sqrt{a^2+b^2}$. With the help of formula (10) we can easily derive the contributions of the epipolar term in $\mathcal{E}(\mathbf{w}, \mathbf{f})$ to the Euler-Lagrange equations. The partial derivative of its integrand $\Psi_e\left((\mathbf{s}^{\top}\mathbf{f})^2\right)$ with respect to $u$ and $v$ are

$$\frac{\partial}{\partial u}\Psi_e\left((\mathbf{s}^{\top}\mathbf{f})^2\right) = 2\,\Psi_e'\left((\mathbf{s}^{\top}\mathbf{f})^2\right)(a\,u + b\,v + q)\,a\,, \tag{11}$$

$$\frac{\partial}{\partial v}\Psi_e\left((\mathbf{s}^{\top}\mathbf{f})^2\right) = 2\,\Psi_e'\left((\mathbf{s}^{\top}\mathbf{f})^2\right)(a\,u + b\,v + q)\,b\,. \tag{12}$$

The contributions from the data term and the smoothness term remain unchanged from the original model. Thus we obtain the final Euler-Lagrange equations of $u$ and $v$ by adding the right hand sides of equations (11) and (12) to the Euler-Lagrange equations given in [3]:

$$\begin{aligned} 0 = \quad & \Psi_d'\left(I_z^2 + \gamma\left(I_{xz}^2 + I_{yz}^2\right)\right)\left(I_x I_z + \gamma\left(I_{xx} I_{xz} + I_{xy} I_{yz}\right)\right) \qquad (13) \\ & - \alpha\,\mathrm{div}\left(\Psi_s'\left(|\nabla u|^2 + |\nabla v|^2\right)\nabla u\right) + \ \beta\,\Psi_e'\left((\mathbf{s}^{\top}\mathbf{f})^2\right)(a\,u + b\,v + q)\ a\,, \\ 0 = \quad & \Psi_d'\left(I_z^2 + \gamma\left(I_{xz}^2 + I_{yz}^2\right)\right)\left(I_y I_z + \gamma\left(I_{yy} I_{yz} + I_{xy} I_{xz}\right)\right) \qquad (14) \\ & - \alpha\,\mathrm{div}\left(\Psi_s'\left(|\nabla u|^2 + |\nabla v|^2\right)\nabla v\right) + \ \beta\,\Psi_e'\left((\mathbf{s}^{\top}\mathbf{f})^2\right)(a\,u + b\,v + q)\ b\,. \end{aligned}$$

Here we have made use of the same abbreviations for the partial derivatives and the temporal differences in the data term as in [3]:

$$\begin{aligned} & I_x \ = \partial_x I(\mathbf{x}+\mathbf{w}), \qquad I_y \ = \partial_y I(\mathbf{x}+\mathbf{w}), \qquad I_z \ = I(\mathbf{x}+\mathbf{w}) - I(\mathbf{x}), \\ & I_{xx} = \partial_{xx} I(\mathbf{x}+\mathbf{w}), \qquad I_{xy} = \partial_{xy} I(\mathbf{x}+\mathbf{w}), \qquad I_{yy} = \partial_{yy} I(\mathbf{x}+\mathbf{w}), \\ & I_{xz} = \partial_x I(\mathbf{x}+\mathbf{w}) - \partial_x I(\mathbf{x}), \qquad I_{yz} = \partial_y I(\mathbf{x}+\mathbf{w}) - \partial_y I(\mathbf{x}). \end{aligned} \tag{15}$$

To differentiate $\mathcal{F}$ with respect to $\mathbf{f}$ we only have to consider the newly introduced epipolar term since neither the data term nor the smoothness term depends on $\mathbf{f}$. The two last equations of (9) give rise to a similar eigenvalue problem as equation (5):

$$\mathbf{0} = \left(\int_{\Omega} \Psi_e'\left((\mathbf{s}^{\top}\mathbf{f})^2\right)\mathbf{s}\mathbf{s}^{\top}\,\mathrm{d}x\,\mathrm{d}y - \lambda I\right)\mathbf{f} = (M - \lambda I)\,\mathbf{f}, \tag{16}$$

$$0 = 1 - \|\mathbf{f}\|^2. \tag{17}$$

Note that we were able to switch the order of differentiation and integration because **f** is a constant over the domain $\Omega$. The system matrix $M$ is symmetric positive definite and its entries are the integral expressions $m_{ij} = \int_\Omega \Psi_e'\left((\mathbf{s}^\top\mathbf{f})^2\right) s_i s_j \,\mathrm{d}x\,\mathrm{d}y$ with $1 \leq i, j \leq 9$ and $s_i$ the $i$-th component of **s**.

### 3.3 Solution of the System of Equations

To solve the system of equations (9) we opt to iterate between the optical flow computation and the fundamental matrix estimation. After solving the Euler-Lagrange equations with a current estimate of the fundamental matrix **f**, we compose the system matrix $M$ based on the computed optical flow **w**. Once $M$ has been retrieved, we solve equation (16) for **f**. Due to the constraint (17) the solution will always be of unit norm. The new estimate of **f** will in turn be used to solve the Euler-Lagrange equations again for **w**, and this process is repeated until convergence. The rank of $F$ is not enforced during this iteration process, but it can be enforced on the final estimate. To solve the Euler-Lagrange equations we adopt the warping strategy proposed in [3]. The flow is incrementally refined on each level of a multiresolution pyramid such that the algorithm does not get trapped in a local minimum. To calculate the flow increment a multigrid solver is used to assure fast convergence. Equation (16) is solved as a series of eigenvalue problems as described in Section 2.

### 3.4 Integrating Data Normalization

We have found the data normalization discussed in Section 2 indispensable in obtaining accurate results. Therefore we have taken the effort to integrate it in our model. The main difficulty in inserting the transformations $T$ and $T'$ into the epipolar constraint $\mathbf{s}^\top\mathbf{f}$ is the dependence of $T' = T'(\mathbf{w})$ on the optical flow. This complicates the derivation of the Euler-Lagrange equations of $u$ and $v$ considerably because the derivative of $T'$ with respect to the flow components has to be taken into account. To overcome this problem we choose $T' = T$. The impact of this simplification is most likely small since the dense point sets of the left and the right image will have a similar distribution. If we employ isotropic scaling as suggested in [8] then $T$ will be a constant transformation only depending on the image domain $\Omega$. As a result substituting $F = T^\top \hat{F}\ T$ in the energy functional does not change the presented Euler-Lagrange equations (13) and (14) in the sense that $a$, $b$ and $q$ are computed from $F$ as before (now via $\hat{F}$). However, replacing the original side constraint $\|F\| = 1$ with $\|\hat{F}\| = 1$ and solving equations (16) and (17) for $\hat{F}$ yields the desired normalization effect during the total least squares fit.

## 4 Experiments

We demonstrate the performance of our method by concentrating on the fundamental matrix estimation and the optical flow computation in two separate experiments. In order to deal with RGB color images we implemented a multichannel variant of our model where the 3 color channels are coupled in the data term as follows

$$\int_\Omega \Psi_d\left(\sum_{i=1}^{3}|I_i(\mathbf{x}+\mathbf{w}) - I_i(\mathbf{x})|^2 + \gamma\cdot\sum_{i=1}^{3}|\nabla I_i(\mathbf{x}+\mathbf{w}) - \nabla I_i(\mathbf{x})|^2\right)\mathrm{d}x\,\mathrm{d}y. \quad (18)$$

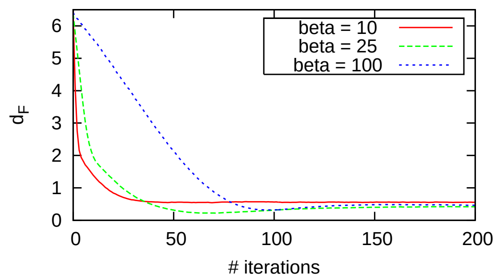


**Fig. 1.** The influence of the parameter $\beta$ on the progression of $d_F$. The experiments were conducted for 1000 iteration steps but convergence takes place within the first 200 steps.

We initialize our method with a zero fundamental matrix such that the first iteration step comes down to the two-step method of recovering the fundamental matrix from pure optical flow [12]. Additionally we exclude those points from the estimation of the fundamental matrix that are warped outside the image. The reason for this is that in these points no data term can be evaluated which has a less reliable flow as result.

In our first experiment we recover the epipolar geometry of a synthetic image pair. The two frames of size $640 \times 480$ represent two views of the 3D reconstruction of a set from a film studio and since they have been generated synthetically the fundamental matrix is known exactly. As an error measure between our estimate for the fundamental matrix and the ground truth we use the distance proposed by Faugeras *et al.* in [5] which we will denote by $d_F$. For this measure two fundamental matrices are used to determine the epipolar lines of several thousand randomly chosen points while systematically switching their roles to assure symmetry. Finally an error measure in pixels is obtained that describes the discrepancy between two epipolar geometries in terms of fundamental matrices for a complete scene. Figure 1 shows how $d_F$ decreases as a function of the number of iterations, and eventually converges. All optical flow parameters have been optimized with respect to the distance error of the first estimated fundamental matrix. We see that the weight $\beta$ has mainly an influence on the convergence speed and to a much lesser extent on the final error. The best results were achieved for $\beta = 25$ with a final error of $d_F = 0.42$ after 1000 iterations. This is significantly below one pixel and a large improvement of the initial error of 6.4 pixels after the first iteration step. The fact that this value is reached after 200 iterations while remaining virtually unchanged afterwards shows the stability of our iteration scheme. In Figure 2 we can observe how an initial estimation of the epipolar line geometry is readjusted during the iteration process to almost coincide with the ground truth. Additionally the initial and the final flow fields are displayed together with the mask for the data term.

In a second experiment we provide evidence that a simultaneous recovery of the epipolar geometry can improve the optical flow estimation substantially. To this end we use our method to compute the optical flow between frames 8 and 9 of the Yosemite sequence without clouds. These two $316 \times 252$ frames actually make up a stereo pair, since only diverging motion is present due to the camera movement. We evaluate the estimated optical flow by means of the average angular error (AAE) [2]. In Table 1 we see that we were able to improve the AAE from $1.59°$ to $1.17°$ and are ranked among the best results published so far for a 2D method. It has to be noted that methods with spatio-temporal smoothness terms give in general slightly smaller errors. For this experiment all optical flow parameters have been optimized with respect to the AAE

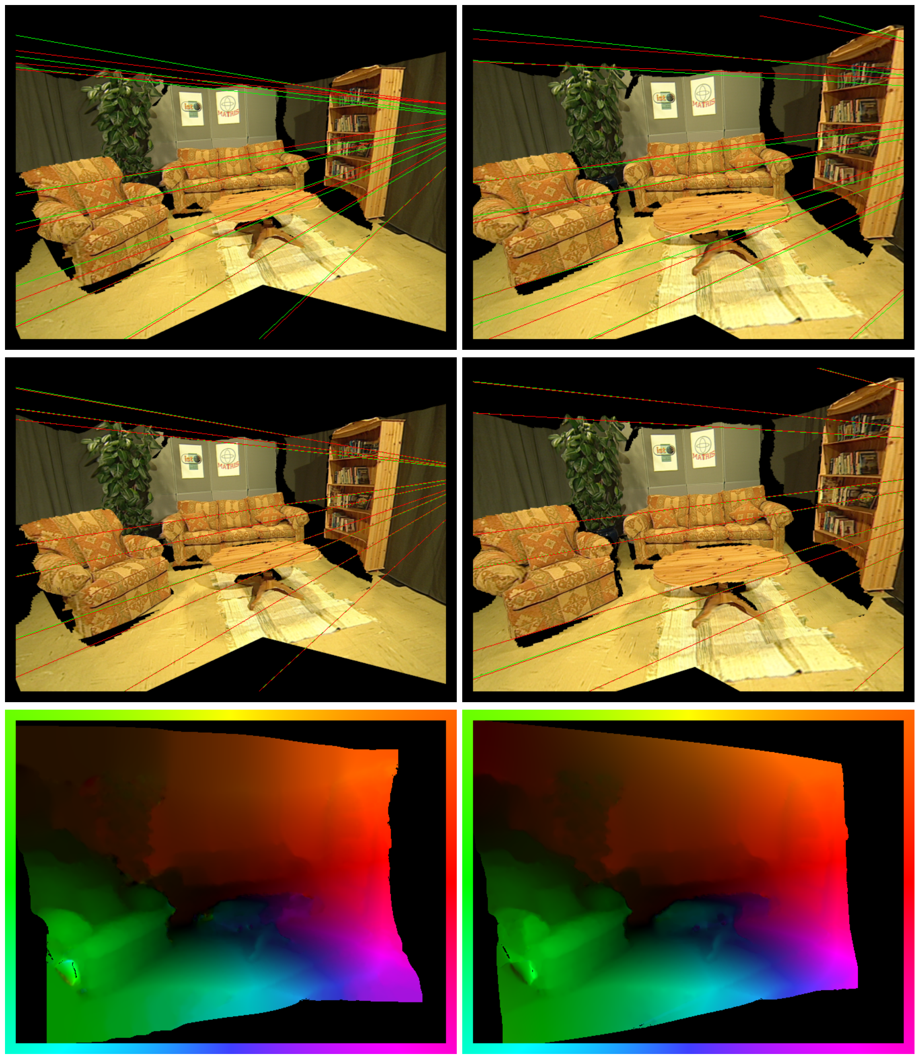

**Fig. 2.** Experiments on a synthetic image sequence. The epipolar lines estimated by our method are depicted as full white lines while the ground truth lines are dotted. **(a) Top Left:** Estimated epipolar lines in the left frame after the first iteration. **(b) Top Right:** Estimated epipolar lines in the right frame after the first iteration. **(c) Middle Left:** Estimated epipolar lines in the left frame after 1000 iterations. **(d) Middle Right:** Estimated epipolar lines in the right frame after 1000 iterations. **(e) Bottom Left:** Magnitude plot of the estimated optical flow field after the first iteration. Brightness encodes magnitude. Pixels that are warped outside the image are colored black. **(f) Bottom Right:** Magnitude plot of the estimated optical flow field after 1000 iterations.

of the first estimated optical flow and $\beta$ has been set to 50. The pixels that are warped outside the image are included in the computation of the AAE. In Figure 3 we show the results for the estimated epipolar lines and flow field. The epipolar lines seem to meet in a common epipole despite the fact that the rank has not been enforced.

**Table 1.** Results for the Yosemite sequence without clouds compared to other 2D methods.

| Method | AAE | Method | AAE |
|---|---|---|---|
| Brox *et al.* [3] | 1.59° | Amiaz *et al.* [1] | 1.44° |
| Mémin/Pérez [13] | 1.58° | Nir *et al.* [14] | 1.18° |
| Roth/Black [15] | 1.47° | **Our method** | **1.17°** |
| Bruhn *et al.* [4] | 1.46° | | |

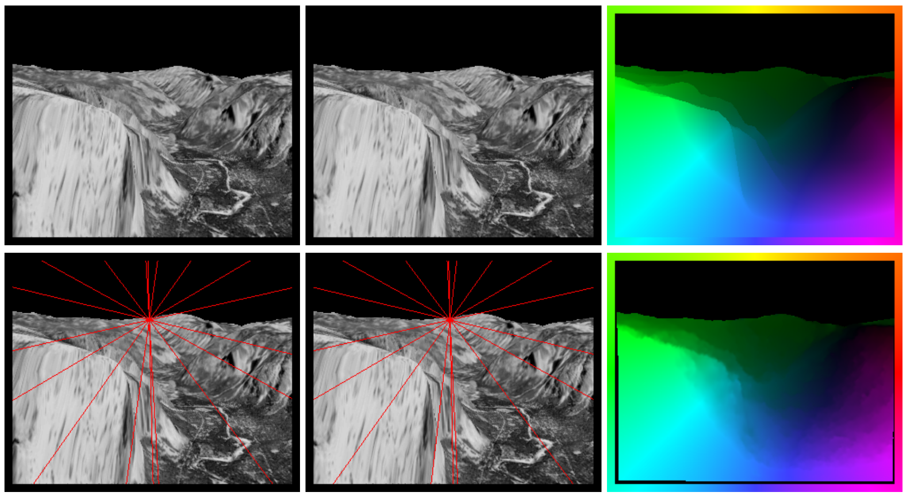

**Fig. 3.** Results for the Yosemite sequence without clouds. **(a) Top Left:** Frame 8. **(b) Top Middle:** Frame 9. **(c) Top Right:** Magnitude plot of the ground truth for the optical flow field between frames 8 and 9. Brightness encodes magnitude. **(d) Bottom Left:** Estimated epipolar lines in frame 8 after 15 iterations. **(e) Bottom Middle:** Estimated epipolar lines in frame 9 after 15 iterations. **(f) Bottom Right:** Magnitude plot of the estimated optical flow after 15 iterations. Pixels (apart from the sky region) that are warped outside the image are colored black.

## 5 Summary

Until now concepts in geometrical and variational computer vision have often been developed independently. In this paper we have demonstrated that two such concepts, namely the estimation of the fundamental matrix and the computation of dense optical flow, can be coupled successfully. To this end we have embedded the epipolar constraint together with a data and smoothness penalty in one energy functional and have proposed an iterative solution method. Experiments not only show the convergence of our scheme but also that the fundamental matrix and the optical flow can be computed very accurately. We hope that these findings will stimulate the efforts to bring together geometrical and variational approaches in computer vision even more.

**Acknowledgements:** Levi Valgaerts gratefully acknowledges funding by the Deutsche Forschungsgemeinschaft (DFG). The authors thank Reinhard Koch and Kevin Köser for providing the film studio image data.

## References


1. T. Amiaz, E. Lubetzky, and N. Kiryati. Coarse to over-fine optical flow estimation. *Pattern Recognition*, 40(9):2496–2503, 2007.
2. J. L. Barron, D. J. Fleet, and S. S. Beauchemin. Performance of optical flow techniques. *International Journal of Computer Vision*, 12(1):43–77, Feb. 1994.
3. T. Brox, A. Bruhn, N. Papenberg, and J. Weickert. High accuracy optic flow estimation based on a theory for warping. In T. Pajdla and J. Matas, editors, *Computer Vision – ECCV 2004*, volume 3024 of *Lecture Notes in Computer Science*, pages 25–36. Springer, Berlin, 2004.
4. A. Bruhn, J. Weickert, and C. Schnörr. Lucas/Kanade meets Horn/Schunck: Combining local and global optic flow methods. *International Journal of Computer Vision*, 61(3):211–231, 2005.
5. O. Faugeras, Q.-T. Luong, and T. Papadopoulo. *The Geometry of Multiple Images*. MIT Press, Cambridge, MA, 2001.
6. M. Fischler and R. Bolles. Random sample consensus: A paradigm for model fitting with applications to image analysis and automated cartography. *Communications of the ACM*, 24:381–385, 1981.
7. R. Hartley and A. Zisserman. *Multiple View Geometry in Computer Vision*. Cambridge University Press, Cambridge, UK, 2000.
8. R. I. Hartley. In defense of the eight-point algorithm. *IEEE Transactions on Pattern Analysis and Machine Intelligence*, 19(6):580–593, 1997.
9. P. J. Huber. *Robust Statistics*. Wiley, New York, 1981.
10. H. C. Longuet-Higgins. A computer algorithm for reconstructing a scene from two projections. *Nature*, 293:133–135, Sept. 1981.
11. Q.-T. Luong and O. D. Faugeras. The fundamental matrix: theory, algorithms, and stability analysis. *International Journal of Computer Vision*, 17(1):43–75, Jan. 1996.
12. M. Mainberger, A. Bruhn, and J. Weickert. Is dense optical flow useful to compute the fundamental matrix? In A. Campilho and M. Kamel, editors, *Image Analysis and Recognition*, Lecture Notes in Computer Science. Springer, Berlin, 2008. To appear.
13. E. Mémin and P. Pérez. Hierarchical estimation and segmentation of dense motion fields. *International Journal of Computer Vision*, 46(2):129–155, 2002.
14. T. Nir, A. M. Bruckstein, and R. Kimmel. Over-parameterized variational optical flow. *International Journal of Computer Vision*, 76(2):205–216, 2008.
15. S. Roth and M. Black. On the spatial statistics of optical flow. In *Proc. Tenth International Conference on Computer Vision*, volume 1, pages 42–49, Beijing, China, June 2005. IEEE Computer Society Press.
16. P. J. Rousseeuw and A. M. Leroy. *Robust Regression and Outlier Detection*. Wiley, New York, 1987.
17. J. Saragih and R. Goecke. Monocular and stereo methods for AAM learning from Video. In *Proc. 2007 IEEE Computer Society Conference on Computer Vision and Pattern Recognition*, pages 1–7, Minneapolis, MN, June 2007. IEEE Computer Society Press.
18. Y. Sheikh, A. Hakeem, and M. Shah. On the direct estimation of the fundamental matrix. In *Proc. 2007 IEEE Computer Society Conference on Computer Vision and Pattern Recognition*, pages 1–7, Minneapolis, MN, June 2007. IEEE Computer Society Press.
19. N. Slesareva, A. Bruhn, and J. Weickert. Optic flow goes stereo: a variational approach for estimating discontinuity-preserving dense dispartiy maps. In W. Kropatsch, R. Sablatnig, and A. Hanbury, editors, *Pattern Recognition*, volume 3663 of *Lecture Notes in Computer Science*, pages 33–40. Springer, Berlin, 2005.